Journal of Materials Chemistry A

RSC Publishing

PAPER

View Article Online
View Journal | View Issue

Cite this: J. Mater. Chem. A, 2013, 1, 2231

ZnO–GaN heterostructured nanosheets for solar energy harvesting: computational studies based on hybrid density functional theory†

Haijun Zhang,[ab] Dihua Wu,[a] Qing Tang,[a] Lu Liu*[a] and Zhen Zhou*[a]

Received 15th October 2012
Accepted 4th December 2012

DOI: 10.1039/c2ta00706a

www.rsc.org/MaterialsA

Through hybrid density functional theory, we computationally designed two-dimensional ZnO–GaN heterostructured nanosheets, and investigated their structural, electronic and optical properties. As a result of the type-II band alignment of ZnO and GaN, both bare $(ZnO)_m(GaN)_n$ and hydrogenated H-$(ZnO)_m(GaN)_n$ (m, $n \geq 3$) nanosheets have band gaps below 3.0 eV with visible-light absorption accordingly, which is confirmed by computed optical properties. Also, photo-induced electrons and holes are directly separated and spatially confined in the ZnO and GaN regions, respectively, which is preferable for restraining ultrafast recombination of photo-excited e^-–h^+ pairs. Moreover, due to the perfect lattice matching of ZnO and GaN crystals, the heterostructured ZnO–GaN nanosheets have few crystal defects at the interfaces, which act as excitons' recombination centres. ZnO–GaN heterostructured nanosheets are promising high-performance materials for solar harvesting.

1 Introduction

It is always a considerable challenge to increase solar utilization efficiency to promote widespread applications of current semiconductor-based photoelectronic devices, such as photocatalysts, and dye- or quantum-dot-sensitized solar cells. A major factor that limits this utilization efficiency is the rapid relaxation of high-energy photo-induced excitons to lower energies and the ultrafast recombination of photogenerated e^-–h^+ pairs, resulting in the conversion of their excess energy to heat through photon emission.[1] After the photoexcitation, most photo-generated electrons and holes are located at the conduction band minimum (CBM) and valence band maximum (VBM) of the semiconductors, respectively. Unfortunately, the photo-induced electrons and holes in conventional materials recombine easily, due to the mixed spatial distribution of their CBM and VBM.[2,3] Efforts have been made to reduce the recombination of activated electron–hole pairs, such as metal/semiconductor composites (Ag/TiO_2,[4] Au/TiO_2,[5] and Pt/TiO_2[6]) and coupled semiconductors (WO_3/TiO_2,[7] SnO_2/TiO_2,[8] ZnO–SnO_2,[9] CdS–TiO_2,[10] and TiO_2/ZnO[11]).

The band offset at the heterojunction of semiconductors generates an effective potential barrier for electrons and holes moving through the interface, which serves as an additional confinement potential for the carriers.[12] The type-I band offset of semiconductor heterostructures results in both electrons and holes being confined in one material, while the type-II leads to a separated distribution of electrons and holes.[13–15] A great number of reports suggest that the type-II heterostructured semiconductors can serve as superior photocatalysts.[16–20] Accordingly, one possible way for simultaneously enhancing efficient charge separation and retarding charge recombination is to adopt heterostructured nanocrystals with staggered type-II band alignment.[17]

However, due to the lattice mismatch, there are many lattice defects at the interface between the coupled semiconductors, which would act as recombination centers for electron–hole pairs and restrict the further application of these composites and coupled semiconductors. The solid solution of gallium/zinc nitride/oxide, $(Ga_{1-x}Zn_x)(N_{1-x}O_x)$, has recently been recognized as a promising photocatalyst for visible-light-driven overall water splitting and pollutant degradation.[21–28] Compared with its wide-band-gap components, the photocatalyst $(Ga_{1-x}Zn_x)(N_{1-x}O_x)$ has a narrower band gap (<3.0 eV) in the visible-light region, due to the type-II band offset of the wurtzite GaN and ZnO semiconductors.[29] Moreover, the difference between the lattice constants of wurtzite GaN ($a = 3.193$ Å, $c = 5.189$ Å) and ZnO ($a = 3.249$ Å, $c = 5.207$ Å) is negligible.[30]

Density functional theory (DFT), the standard tool in modern condensed matter physics, is plagued by one serious shortcoming. As is well known, the Kohn–Sham (KS) band gaps of

[a]Key Laboratory of Advanced Energy Materials Chemistry (Ministry of Education), Tianjin Key Laboratory of Environmental Remediation and Pollution Control, Computational Centre for Molecular Science, Institute of New Energy Material Chemistry, Nankai University, Tianjin 300071, P. R. China. E-mail: liul@nankai.edu.cn; zhouzhen@nankai.edu.cn

[b]School of Physics and Materials Science, Anhui University, Hefei 230039, P. R. China

† Electronic supplementary information (ESI) available. See DOI: 10.1039/c2ta00706a

DFT are systematically underestimated by 50%–100% of the experimental ones. In particular, the KS band gaps of ZnO and GaN almost vanish, in contrast to their experimental values of 3.2 eV and 3.4 eV,[31–33] respectively. The main reason for this failure is that both local density approximation (LDA) and generalized gradient approximation (GGA) are jellium-based exchange-correlation (XC) energy functionals that suffer from (i) an incomplete cancellation of the artificial Hartree self-interaction and (ii) the lack of the integer discontinuity in the exchange and correlation energy upon adding an electron.[34] An alternative to the conventional (semi) local XC functional is the hybrid density functional. Among numerical hybrid functionals, such as PBE0, B3LYP and B3PW91, the recently developed Heyd–Scuseria–Ernzerhof (HSE) functional has proved an outstanding method to predict the band gaps of semiconductors, especially the band gaps of ZnO and GaN.[34–36] Very recently, Zhao's group have investigated the band alignment and optical properties of ZnO–GaN and ZnO–$(Ga_{1-x}Zn_x)(N_{1-x}O_x)$–GaN heterostructures using HSE functionals.[37] Herein, through the screened hybrid density functional HSE06 computations, we investigated the structural, electronic and optical properties of two-dimensional (2D) ZnO–GaN heterostructured nanosheets, which show attractive properties for solar harvesting. For comparison, we also investigated the energy and geometry of CdSe–CdTe heterostructured nanosheets as an example, to disclose the formation of lattice defects at the interface of the coupled semiconductors.

2 Computational details

The computations were performed within the projector-augmented plane wave (PAW) approach[38,39] as implemented in the Vienna *ab initio* simulation package (VASP).[40] The structure optimization, and the computations of band structures and density of states (DOS) were performed by using the screened hybrid density functional HSE06. The screening parameter μ in HSE was fixed at a value of 0.2 $Å^{-1}$ and the mixing parameter α was set as 0.36.[35] The tolerance for energy convergence was set to be 10^{-4} eV, while the ionic relaxation was converged when the force on the atoms was smaller than 10^{-3} eV $Å^{-1}$. The Brillouin zone was integrated by using Monkhorst–Pack generated sets of k points. The structures of GaN and ZnO belong to the hexagonal space group $P63mc$ (no. 186). In this work, experimental lattice parameters were adopted as the starting points, and both atomic positions and lattice constants were optimized in the bulk structure. For the purpose of comparative analysis and resource economization, only $(GaN)_{0.5}(ZnO)_{0.5}$ was considered for the bulk alloyed structure. The $4 \times 4 \times 4$ k-point mesh and $2 \times 2 \times 2$ supercell were benchmarked to be sufficient to reach the convergence for bulk optimization. Band structures of bulk materials were computed along the special lines connecting the following high-symmetry points: Z (0, 0, 0.5), L (0.5, 0, 0.5), M (0.5, 0, 0), G (0, 0, 0), Z (0, 0, 0.5), H (0.333, 0.333, 0.5), K (0.333, 0.333, 0), and G (0, 0, 0) in the k-space. The computations on 2D nanosheets were performed by using the slab model, in which a finite number of crystal layers in a three-dimensional (3D) periodic cell were used to generate the nanosheets *via* the introduction of a vacuum gap. In spite of the high surface activities, the polar (0001) surfaces of ZnO and GaN exhibit metallic and deep p-type or n-type properties,[41–44] respectively, which are detrimental to photocatalysis or other photo-voltaic processes.[45] Accordingly, all nanosheets are constructed from a 3D wurtzite structure and terminated with non-polar $(10\bar{1}0)$, as depicted in Fig. 1. For convenience, we labeled the bare (hydrogenated) nanosheets with m layer ZnO and n layer GaN as $(ZnO)_m(GaN)_n$ (H-$(ZnO)_m(GaN)_n$). The vacuum gap of 15 Å is large enough that interactions between the periodic images perpendicular to the surface are negligible. A $3 \times 3 \times 1$ k-point grid was used for the sheet relaxation, with the third vector perpendicular to the $(10\bar{1}0)$ surface. On the basis of fully relaxed slabs, band structures were computed along the special lines connecting the following high-symmetry points: G (0, 0, 0), M (0.5, 0, 0), K (0.333, 0.333, 0) and G (0, 0, 0) in the k-space.

3 Results and discussion

The HSE06 optimized lattice parameters of ZnO (GaN) are a = 3.25 Å and c = 5.20 Å (a = 3.19 Å and c = 5.19 Å), which agree well with other HSE results and experimental values.[30–36] To investigate the electronic properties and optical absorption, we computed the band structures of the bulk ZnO and GaN by using the HSE functional. As shown in Fig. 2, both the bulk ZnO and GaN have direct band gaps at the G point. The band gaps of ZnO and GaN are 3.23 eV and 3.47 eV, respectively, which are also consistent with other HSE results[34–36] and experimental values.[32–34] Obviously, both ZnO and GaN do not have visible-light absorption spectra, resulting in the drawback of these photovoltaic semiconductors. Many reports have suggested that the solid solution of gallium/zinc nitride/oxide, $(Ga_{1-x}Zn_x)(N_{1-x}O_x)$, is a promising photocatalyst for visible-light-driven overall water splitting and pollutant degradation.[21,22] It is of value to investigate the band structures of the

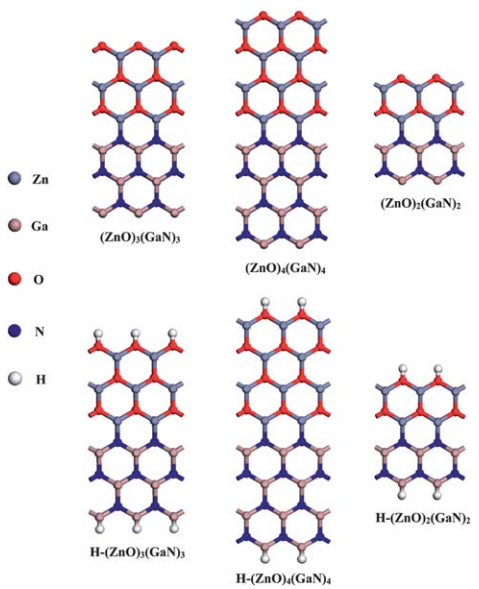

Fig. 1 Bare and hydrogenated ZnO–GaN nanosheets with $(10\bar{1}0)$ surface.

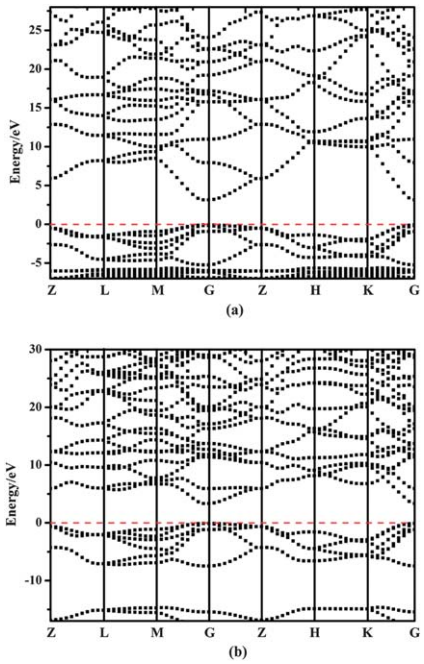

Fig. 2 Band structures of (a) ZnO and (b) GaN. Red dashed lines represent the Fermi level at 0 eV.

alloyed ZnO and GaN, *i.e.* the $(Ga_{1-x}Zn_x)(N_{1-x}O_x)$ compounds, to clarify the results of many experimental and computational studies. Through the HSE06 computations of bulk $(Ga_{0.5}Zn_{0.5})(N_{0.5}O_{0.5})$, we obtained a band gap of 2.22 eV, corresponding to the visible spectrum wavelength of about 560 nm, which also agrees well with the experimental values (2.2 eV–2.4 eV).[25,27] Therefore, the hybrid density functional HSE06 is suitable for computing the electronic properties of ZnO, GaN, and their corresponding alloys. Additionally, the $(Ga_{1-x}Zn_x)(N_{1-x}O_x)$ compounds with particular nanostructures may be potential photovoltaic materials for solar harvesting.

As mentioned above, the $(ZnO)_m(GaN)_n$ nanosheets with particular structures may have novel characteristics for solar harvesting. The band structures of the bare and hydrogenated $(ZnO)_2(GaN)_2$, $(ZnO)_3(GaN)_3$ and $(ZnO)_4(GaN)_4$ nanosheets are shown in Fig. 3. All the nanosheets have direct band gaps at the *G* point. As a result of the quantum size effect, the $(ZnO)_4(GaN)_4$ nanosheets have the smallest band gap and the following sequence is $(ZnO)_3(GaN)_3$ < $(ZnO)_2(GaN)_2$ (see Fig. 3a–c). Extraordinarily, all bare nanosheets have band gaps smaller than 3.0 eV, indicating optical absorption in the visible light spectrum.

With respect to the surface effect, the experimental operability and the environmental stability, we also considered hydrogenated nanosheets. As expected, the hydrogenated $(ZnO)_2(GaN)_2$, $(ZnO)_3(GaN)_3$ and $(ZnO)_4(GaN)_4$ nanosheets have larger band gaps than their corresponding bare ones (see Fig. 3d–f). The band gaps of the hydrogenated nanosheets have the sequence: H-$(ZnO)_2(GaN)_2$ > H-$(ZnO)_3(GaN)_3$ > H-$(ZnO)_4(GaN)_4$, also due to the quantum size effect. Significantly, the H-$(ZnO)_3(GaN)_3$ and H-$(ZnO)_4(GaN)_4$ nanosheets have band gaps of 2.99 eV and 2.64 eV, respectively, implying their

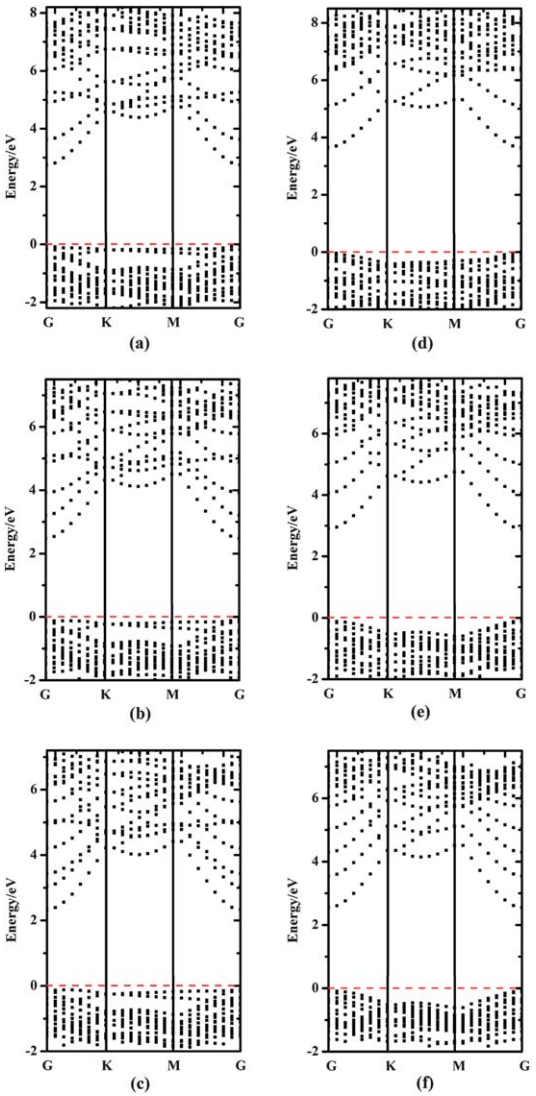

Fig. 3 (a–c) and (d–f) show the band structures of the bare and hydrogenated $(ZnO)_m(GaN)_n$ ($m = n = 2, 3, 4$) nanosheets, respectively. Red dashed lines represent the Fermi level at 0 eV.

visible-light absorption. The band gaps of both the bare and hydrogenated nanosheets decrease with increasing the thickness of the nanosheets, as shown in Fig. 3. Therefore, the passivated ZnO–GaN heterostructured nanosheets, with more than 3 layers of both ZnO and GaN ($m = n \geq 3$), should have visible-light absorption and the potential for efficient solar harvesting.

To investigate the band structures of the heterostructured nanosheets with geometrically asymmetric layers, we also computed the band structures of the bare and hydrogenated $(ZnO)_m(GaN)_n$ ($m, n = 2, 3, 4$, and $m \neq n$) nanosheets, and their band gaps are listed in Table 1. All the bare $(ZnO)_m(GaN)_n$ nanosheets have band gaps below 3.0 eV, due to the abundant dangling bonds at the nanosheet surfaces. Compared with those of the $(ZnO)_m(GaN)_n$ nanosheets, the band gaps of the H-$(ZnO)_m(GaN)_n$ nanosheets increase a lot, resulting from the passivation of the surface dangling bonds. All the thin

Table 1 Band gaps of $(ZnO)_m(GaN)_n$ and H-$(ZnO)_m(GaN)_n$ (m, n = 2, 3, 4 and $m \neq n$) nanosheets

Nanosheets	Band gaps (eV)
$(ZnO)_2(GaN)_3$/H-$(ZnO)_2(GaN)_3$	2.80/3.42
$(ZnO)_3(GaN)_2$/H-$(ZnO)_3(GaN)_2$	2.61/3.59
$(ZnO)_2(GaN)_4$/H-$(ZnO)_2(GaN)_4$	2.82/3.28
$(ZnO)_4(GaN)_2$/H-$(ZnO)_4(GaN)_2$	2.52/2.87
$(ZnO)_3(GaN)_4$/H-$(ZnO)_3(GaN)_4$	2.55/2.91
$(ZnO)_4(GaN)_3$/H-$(ZnO)_4(GaN)_3$	2.49/2.75

passivated nanosheets have band gaps above 3.2 eV. Similar to the bare nanosheets, the band gaps of the hydrogenated nanosheets decrease with increasing their thickness. As listed in Table 1, the H-$(ZnO)_3(GaN)_4$ and H-$(ZnO)_4(GaN)_3$ nanosheets have band gaps of 2.91 eV and 2.75 eV, respectively. In spite of the geometrically asymmetric layers, these ZnO–GaN heterostructured nanosheets with appropriate thickness (m, $n \geq 3$, and $m \neq n$) should still have band gaps below 3.0 eV and, thus, can absorb visible light.

The optical absorption properties of pure ZnO, GaN and alloyed $(Ga_{0.5}Zn_{0.5})(N_{0.5}O_{0.5})$ were also investigated by computing the complex dielectric constants at a given frequency ω, which can be defined as $\varepsilon(\omega) = \varepsilon_1(\omega) + i\varepsilon_2(\omega)$. The expression for the absorption coefficient $I(\omega)$ was given as:[46]

$$I(\omega) = \sqrt{2}\omega\left[\sqrt{\varepsilon_1(\omega)^2+\varepsilon_2(\omega)^2} - \varepsilon_1(\omega)\right]^{1/2} \quad (1)$$

As shown in the equation, only if the imaginary part $\varepsilon_2(\omega) > 0$, the absorption coefficient $I(\omega)$ will be above zero. Accordingly, the imaginary part reflects the absorption coefficient at a given frequency ω. The imaginary part can be written as:[37,47]

$$\varepsilon^{(2)}_{\alpha\beta}(\omega) = \frac{4\pi^2e^2}{\Omega}\lim_{q\to 0}\frac{1}{q^2}\sum_{c,v,\vec{k}} 2w_{\vec{k}}\,\delta\left(\varepsilon_{c\vec{k}} - \varepsilon_{v\vec{k}} - \omega\right) \times \left\langle u_{c\vec{k}+e_\alpha\vec{q}}\middle| u_{v\vec{k}}\right\rangle\left\langle u_{c\vec{k}+e_\beta\vec{q}}\middle| u_{v\vec{k}}\right\rangle^* \quad (2)$$

where the indices c and v are restricted to the conduction and valence band states, respectively, which were determined from the HSE06 functional, and $u_{c\vec{k}}$ is the cell periodic part of the wavefunctions at the k-point.

For the accurate computation of optical properties, we employed the 8 × 8 × 8 and 10 × 10 × 4 k-point mesh for the bulk and slab models and present the imaginary part of dielectric constants for these structures in Fig. 4. The $\varepsilon_2(\omega)$ term of the three bulk materials is composed of two components, $\varepsilon_{zz}(\omega)$ and $\varepsilon_{xy}(\omega)$, which are the components parallel and perpendicular to the z direction, respectively. We can see from Fig. 4 that there are two obvious absorption peaks at about 2.36 eV and 2.79 eV for the alloyed $(Ga_{0.5}Zn_{0.5})(N_{0.5}O_{0.5})$, resulting from the band alignment between the ZnO and GaN host materials. Due to the high computational demands, we only computed the complex dielectric functions of the H-$(ZnO)_4$-$(GaN)_4$ model for simplicity. Similarly, as shown in Fig. S1

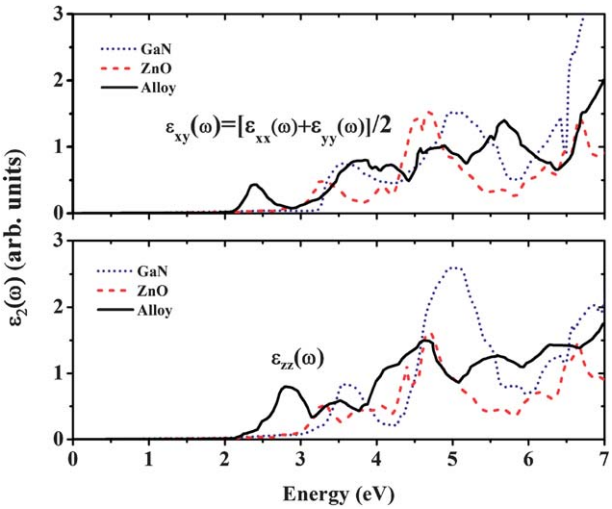

Fig. 4 Imaginary parts of GaN, ZnO, and $(Ga_{0.5}Zn_{0.5})(N_{0.5}O_{0.5})$.

(ESI†), H-$(ZnO)_4(GaN)_4$ has absorption peaks at 2.80 eV and 3.01 eV, which are also in the visible region. The evidence of the absorption peaks in the visible light region validates the implication of band structures, and accordingly manifests the potential application for high-performance solar harvesting.

Besides the significant superiority of visible-light absorption, the type-II band offset of GaN and ZnO leads to directly separated distribution of electrons and holes in GaN–ZnO heterostructures.[23,29] To investigate the charge distribution of these novel ZnO–GaN heterostructured nanosheets, we computed the density of states (DOS) and projected local DOS for the $(ZnO)_m(GaN)_n$ and H-$(ZnO)_m(GaN)_n$ (m, n = 2, 3, 4) nanosheets (Fig. 5). Due to the quantum confinement effect, the separation of the CBM for GaN and ZnO is not clear in $(ZnO)_2(GaN)_2$ and H-$(ZnO)_2(GaN)_2$. For the nanosheets with more than three layers of ZnO and GaN (m, $n \geq 3$), the CBM and VBM are mainly located in the ZnO and GaN regions, respectively. With increasing layers of nanosheets, the boundaries of the band edges tend to be clearer. Significantly, the distributions of the band edges are almost unaffected by the surface passivation. Considering the nanosheets with geometrically asymmetric layers, we present the projected local DOS of the bare and hydrogenated $(ZnO)_3(GaN)_4$ and $(ZnO)_4(GaN)_3$ nanosheets as examples, as shown in Fig. 6. The CBM and VBM of the nanosheets with asymmetric layers are also contributed by the ZnO and GaN components, respectively. Additionally, we also computed the spatial locations of the CBM and VBM at the G point for the investigated nanosheets and present them in Fig. S2 and S3 (ESI†), which agree well with DOS. In other words, the photo-induced electrons and holes within these photo-excited ZnO–GaN nanosheets are directly separated and confined in the ZnO and GaN regions, respectively.

After full relaxation of the atomic positions, there is a little inward and outward motion of surface Ga (Zn) and N (O) atoms, respectively, as a result of the surface reconstruction within all investigated 2D GaN–ZnO nanosheets. Obviously, within these nanosheets, there are unusual Ga–O and Zn–N bonds at the

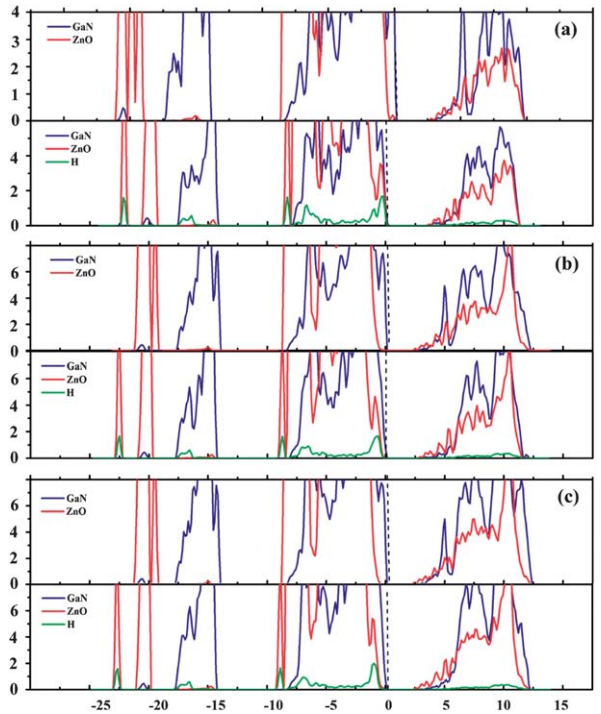

Fig. 5 (a–c) Projected local DOS for bare (upper) and hydrogenated (lower) $(ZnO)_m(GaN)_n$ ($m = n = 2, 3, 4$) nanosheets, respectively. Black dashed lines represent the interface between the ZnO and GaN regions.

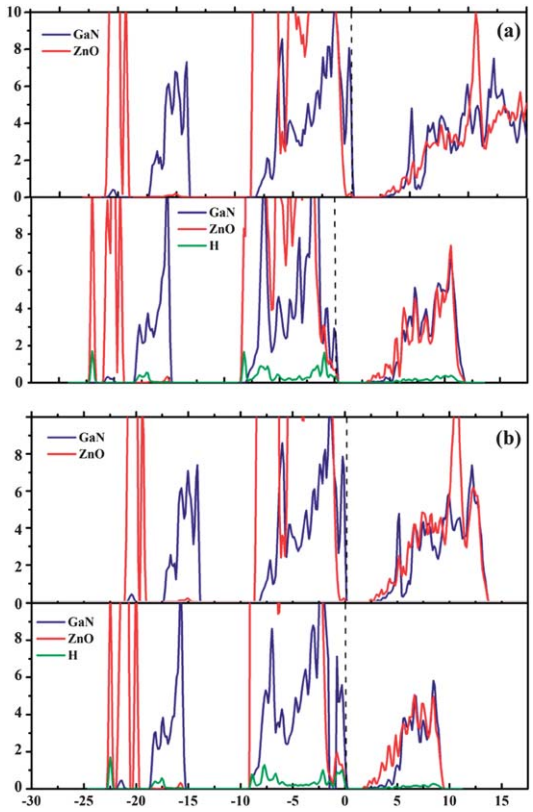

Fig. 6 Projected local DOS of bare (upper) and passivated (lower) $(ZnO)_3(GaN)_4$ (a) and $(ZnO)_4(GaN)_3$ (b) nanosheets. Black dashed lines represent the interface between the ZnO and GaN regions.

interface between the coupled GaN and ZnO semiconductors. Due to the slight lattice mismatch, the difference between the Ga–N (Zn–O) and Ga–O (Zn–N) bonds is neglectable. For example, with respect to the $(ZnO)_3(GaN)_3$ nanosheets, the average difference between the Ga–N (Zn–O) and Ga–O (Zn–N) bonds is 0.06 Å (0.04 Å).

To clarify how the lattice mismatch affects the structural stability and interface defects of the investigated nanosheets, we calculated the formation energies of pure, alloyed, and heterostructured ZnO–GaN nanosheets with m' and n' Zn–O and Ga–N pairs, respectively. The formation energy (E_f) is defined as:[48]

$$E_f = (E_{tot} - mE_{ZnO} - nE_{GaN})/(m' + n') \quad (3)$$

where E_{ZnO} and E_{GaN} are the energies of one Zn–O pair in the wurtzite ZnO bulk and one Ga–N pair in the wurtzite GaN bulk, respectively, E_{tot} is the total energy of the investigated nanosheet, and m' and n' are the total number of Zn–O and Ga–N pairs in the ZnO–GaN nanosheets, respectively.

In view of the reliability of our computations, we first computed small models with 12 Zn–O and 12 Ga–N pairs, by employing both the HSE06 and standard DFT methods. HSE06 and PBE give similar geometries and energies. Additionally, we compared the energies of the ZnO–GaN heterostructured nanosheets with (2×1), (2×2) and (3×3) surfaces with the formation energies of 0.101 eV, 0.229 eV and 0.233 eV, respectively. Therefore, the (2×2) surface is large enough to give a reasonable description for strain energy and lattice mismatch.

In our computations, the pure ZnO and GaN nanosheets are composed of 48 Zn–O and Ga–N pairs, respectively. For alloyed and heterostructured nanosheets, only the nanosheets with 24 Zn–O and 24 Ga–N pairs were considered. Note that the alloyed nanosheets with different configurations have different formation energies. Therefore, we computed five alloyed nanosheets with different configurations, and chose the most energetically favorable one for further comparison.

As listed in Table 2, for the GaN–ZnO nanosheets, the E_f of heterostructured nanosheets is between those of pure ZnO and GaN nanosheets and much lower than that of the alloyed nanosheets, which indicates a more harmonic crystal structure and higher thermodynamic stability of the heterostructured nanosheets. To compare the GaN–ZnO heterostructured nanosheets with other type-II-band-offset semiconductors, which can also be used for solar harvesting,[17] we calculated the formation energies of CdTe–CdSe nanosheets with the same geometry. We can see from the relaxed CdSe and CdTe supercells that the Cd–Se and Cd–Te bonds are 2.68 Å and 2.86 Å,

Table 2 Formation energies, E_f (in eV) of the GaN–ZnO and CdSe–CdTe nanosheets with pure, alloyed, and heterojunction structures

	Pure	Heterojunction	Alloy
ZnO–GaN	0.163/0.295	0.229	0.421
CdTe–CdSe	0.060/0.074	0.115	0.099

respectively. For the alloyed and heterostructured CdSe–CdTe nanosheets, the average difference between the Cd–Se and Cd–Te bonds is 0.17 Å, resulting in severe lattice mismatch at the interface of the coupled CdSe–CdTe nanosheets. Therefore, the heterostructured CdTe–CdSe nanosheets have the highest formation energies, as listed in Table 2.

To further clarify the interface effects on the crystal defects of the heterostructured ZnO–GaN (CdTe–CdSe) nanosheets, we should eliminate the surface dangling bonds and compare their energetic properties. Accordingly, we suppose that the heterostructured ZnO–GaN (CdTe–CdSe) nanosheet is a combination of half pure ZnO (CdTe) and half pure GaN (CdSe) nanosheets, with only one of the $(10\bar{1}0)$ surfaces exposed. We also give a definition for *D*-value ($\Delta_{ZnO-GaN}$) to compare the energetic properties of pure and heterostructured nanosheets. Taking the heterostructured ZnO–GaN nanosheet as an example, its *D*-value is defined as:

$$\Delta_{ZnO-GaN} = E_h - (E_{ZnO} + E_{GaN})/2 \quad (4)$$

where E_h is the total energy of the heterostructured ZnO–GaN nanosheets, E_{ZnO} and E_{GaN} are the energies of the pure ZnO and GaN nanosheets, respectively. All the nanosheets have the same number of atoms and layers. According to the calculation, we obtain *D*-values of −0.023 eV and 3.427 eV for the heterostructured ZnO–GaN and CdTe–CdSe nanosheets, respectively. Compared with CdSe–CdTe nanosheets with the same geometry, the *D*-value of the heterostructured ZnO–GaN nanosheets is almost zero and negligible. Accordingly, the heterostructured ZnO–GaN nanosheets are energetically favorable, which results from its better matched crystal lattice at the interface. Lattice defects at the interface of the coupled semiconductors should act as the recombination centers of the electron–hole pairs and restrict the further applications of these types of heterojunction semiconductors.[49–51] Therefore, compared with other type-II-band-offset semiconductors, the heterostructured ZnO–GaN nanosheets with better matched interface and fewer interface defects are more preferable for photo-catalytic and photovoltaic applications.

4 Conclusion

In summary, through hybrid density functional computations, we designed 2D ZnO–GaN heterostructured nanosheets, and investigated their structural, electronic and optical properties. Both bare $(ZnO)_m(GaN)_n$ and hydrogenated H-$(ZnO)_m(GaN)_n$ nanosheets with appropriate thickness (m, $n \geq 3$) have band gaps smaller than 3.0 eV, indicating the visible-light absorption of these novel nanosheets. Remarkably, the heterostructured ZnO–GaN nanosheets have spatial distributions of CBMs and VBMs mainly located in ZnO and GaN regions, respectively, which leads to the direct separation and spatial confinement of the photo-induced e^-–h^+ pairs. Moreover, compared with other type-II-band-offset coupled semiconductors, there are fewer crystal defects at the interface of the coupled semiconductors, as a result of the lattice matching of the ZnO and GaN crystals. With high stability, a defect-free interface, direct separation and spatial confinement of the e^-–h^+ pairs, as well as their visible-light absorption, ZnO–GaN heterostructured nanosheets are promising high-efficiency materials for solar harvesting.

Acknowledgements

This work was supported by Tianjin Municipal Science and Technology Commission (12JCZDJC28100) and Fundamental Research Funds for the Central Universities. The computations were performed on TianHe-1(A) at the National Supercomputer Center in Tianjin and Magic Cube at Shanghai Supercomputer Center.

Notes and references

1 N. S. Lewis, *Science*, 2007, **315**, 798.
2 Y. J. Wang, R. Shi, J. Lin and Y. F. Zhu, *Energy Environ. Sci.*, 2011, **4**, 2922.
3 H. J. Zhang, G. H. Chen and D. W. Bahnemann, *J. Mater. Chem.*, 2009, **19**, 5089.
4 T. Hirakawa and P. V. Kamat, *J. Am. Chem. Soc.*, 2005, **127**, 3928.
5 M. Jakob, H. Levanon and P. V. Kamat, *Nano Lett.*, 2003, **3**, 353.
6 M. A. Fox and M. T. Dulay, *Chem. Rev.*, 1993, **93**, 341.
7 J. Papp, S. Soled, K. Dwight and A. Wold, *Chem. Mater.*, 1994, **6**, 496.
8 K. Vinodgopal and P. V. Kamat, *Environ. Sci. Technol.*, 1995, **29**, 841.
9 M. Zhang, T. An, X. Hu, C. Wang, G. Sheng and J. Fu, *Appl. Catal., A*, 2004, **260**, 215.
10 A. Kumar and A. K. Jain, *J. Mol. Catal. A: Chem.*, 2001, **165**, 265.
11 R. S. Mane, W. J. Lee, H. M. Pathan and S.-H. Han, *J. Phys. Chem. B*, 2005, **109**, 24254.
12 M. S. Gudiksen, L. J. Lauhon, J. Wang, D. C. Smith and C. M. Lieber, *Nature*, 2002, **415**, 617.
13 A. Nduwimana, R. N. Musin, A. M. Smith and X. Q. Wang, *Nano Lett.*, 2008, **8**, 3341.
14 H. J. Zhang, Y. F. Li, Q. Tang, L. Liu and Z. Zhou, *Nanoscale*, 2012, **4**, 1078.
15 Z. Liu, J. Wu, W. H. Duan, M. G. Lagally and F. Liu, *Phys. Rev. Lett.*, 2010, **105**, 016802.
16 I. Gur, N. A. Fromer, M. L. Geier and A. P. Alivisatos, *Science*, 2005, **310**, 462.
17 H. M. Zhu, N. H. Song and T. Q. Lian, *J. Am. Chem. Soc.*, 2011, **133**, 8762.
18 S. Z. Wang and L. W. Wang, *J. Phys. Chem. Lett.*, 2011, **2**, 1.
19 M. Jones, S. Kumar, S. S. Lo and G. D. Scholes, *J. Phys. Chem. C*, 2008, **112**, 5423.
20 S. D. Singh, V. K. Dixit, S. Porwal, R. Kumar, A. K. Srivastava, T. Ganguli, T. K. Sharma and S. M. Oak, *Appl. Phys. Lett.*, 2010, **97**, 111912.
21 D. L. Lu, T. Takata, N. Saito, Y. Inoue and K. Domen, *Nature*, 2006, **440**, 295.
22 K. Maeda, T. Takata, M. Hara, N. Saito, Y. Inoue, H. Kobayashi and K. Domen, *J. Am. Chem. Soc.*, 2005, **127**, 8286.

23 S. Z. Wang and L. W. Wang, *Phys. Rev. Lett.*, 2010, **104**, 065501.
24 M. Yashima, H. Yamada, K. Maeda and K. Domen, *Chem. Commun.*, 2010, **46**, 2379.
25 K. Maeda and K. Domen, *Chem. Mater.*, 2010, **22**, 612.
26 W. Q. Han, Y. Zhang, C.-Y. Nam, C. T. Black and E. E. Mendez, *Appl. Phys. Lett.*, 2010, **97**, 083108.
27 W. Q. Han, Z. X. Liu and H. G. Yu, *Appl. Phys. Lett.*, 2010, **96**, 183112.
28 J. H. Kou, Z. S. Li, Y. Guo, J. Gao, M. Yang and Z. G. Zou, *J. Mol. Catal. A: Chem.*, 2010, **325**, 48.
29 M. N. Huda, Y. F. Yan, S. H. Wei and M. M. Al-Jassim, *Phys. Rev. B: Condens. Matter Mater. Phys.*, 2008, **78**, 195204.
30 Y. N. Xu and W. Y. Ching, *Phys. Rev. B: Condens. Matter*, 1993, **48**, 4335.
31 D. Vogel, P. Krüger and J. Pollmann, *Phys. Rev. B: Condens. Matter*, 1995, **52**, R14316.
32 D. C. Reynolds, D. C. Look, B. Jogai, C. W. Litton, G. Cantwell and W. C. Harsch, *Phys. Rev. B: Condens. Matter*, 1999, **60**, 2340.
33 H. Teisseyre, P. Perlin, T. Suski, I. Grzegory, S. Porowski and J. Jun, *J. Appl. Phys.*, 1994, **76**, 2429.
34 J. Wróbel, K. J. Kurzydłowski, K. Hummer, G. Kresse and J. Piechota, *Phys. Rev. B: Condens. Matter Mater. Phys.*, 2009, **80**, 155124.
35 F. Oba, A. Togo, I. Tanaka, J. Paier and G. Kresse, *Phys. Rev. B: Condens. Matter Mater. Phys.*, 2008, **77**, 245202.
36 Y. F. Duan, L. X. Qin, L. W. Shi, G. Tang and H. L. Shi, *Appl. Phys. Lett.*, 2012, **100**, 022104.
37 Z. H. Wang, M. W. Zhao, X. P. Wang, Y. Xi, X. J. He, X. D. Liu and S. S. Yan, *Phys. Chem. Chem. Phys.*, 2012, **14**, 15693.
38 P. E. Blöchl, *Phys. Rev. B: Condens. Matter*, 1994, **50**, 17953.
39 G. Kresse and D. Joubert, *Phys. Rev. B: Condens. Matter Mater. Phys.*, 1999, **59**, 1758.
40 G. Kresse and J. Hafner, *Phys. Rev. B: Condens. Matter*, 1994, **49**, 14251.
41 B. Meyer and D. Marx, *Phys. Rev. B: Condens. Matter*, 2003, **67**, 035403.
42 N. Sanchez, S. Gallego, J. Cerdá and M. C. Muñoz, *Phys. Rev. B: Condens. Matter Mater. Phys.*, 2010, **81**, 115301.
43 P. Kempisty, P. Strąk and S. Krukowski, *Surf. Sci.*, 2011, **605**, 695.
44 Q. Tang, Y. Cui, Y. F. Li, Z. Zhou and Z. F. Chen, *J. Phys. Chem. C*, 2011, **115**, 1724.
45 X. G. Ma, B. Lu, D. Li, R. Shi, C. S. Pan and Y. F. Zhu, *J. Phys. Chem. C*, 2011, **115**, 4680.
46 S. Saha and T. P. Sinha, *Phys. Rev. B: Condens. Matter*, 2000, **62**, 8828.
47 M. Gajdoš, K. Hummer and G. Kresse, *Phys. Rev. B: Condens. Matter Mater. Phys.*, 2006, **73**, 045112.
48 H. B. Shu, X. S. Chen, H. X. Zhao, X. H. Zhou and W. Lu, *J. Phys. Chem. C*, 2010, **114**, 17514.
49 I. Tsuji, H. Kato, H. Kobayashi and A. Kudo, *J. Am. Chem. Soc.*, 2004, **126**, 13406.
50 H. Kato, H. Kobayashi and A. Kudo, *J. Phys. Chem. B*, 2002, **106**, 12441.
51 H. J. Zhang, L. Liu and Z. Zhou, *RSC Adv.*, 2012, **2**, 9224.